Water Supply

IWA PUBLISHING

Water Supply Vol 22 No 1, 126 doi: 10.2166/ws.2021.280

Layer-by-layer self-assembly preparation and desalination performance of graphene oxide membrane

Jun Hu and Zuoguo Yang*

School of Chemical Engineering, East China University of Science and Technology, 130 Meilong Road, Xuhui District, Shanghai, China
*Corresponding author. E-mail: zgyang@ecust.edu.cn

JH, 0000-0001-6579-1323; ZY, 0000-0002-1606-192X

ABSTRACT

Unlike previous utilization of ultrafiltration membranes as supporters of graphene oxide (GO) composite membranes, this study first adopts microporous nylon membranes as substrates. The cationic polyelectrolyte/GO composite membranes are prepared by the layer-by-layer self-assembly method via electrostatic attraction. The introduction of polycations between nanochannels in the GO membranes effectively suppresses the swelling and improves the stability of the membranes. It is found that the polyelectrolytes' charge density and the surface potential of the composite membranes jointly determine the membranes' properties. The experimental results show that the novel GO membranes can obtain high flux and considerable desalination performance under low operating pressure. Typically, the salt rejection rate reaches 66.8% for 1.0 g/L $MgSO_4$, and the flux is 39.8 $L{\cdot}m^{-2}{\cdot}h^{-1}{\cdot}bar^{-1}$. Benefitting from the GO composite membranes keeping similar retention for both high and low concentration salt solutions, the ideal desalination performance could be obtained through multi-stage processes on the premise of ensuring high flux, which is more suitable for industry.

Key words: graphene oxide, layer-by-layer assembly, membrane separation, nanofiltration, polyelectrolyte

HIGHLIGHTS

- Cationic polyelectrolyte/graphene oxide composite membranes were firstly prepared by layer-by-layer self-assembly via electrostatic attraction on the nylon microfiltration membranes.
- High flux and considerable desalination performance were obtained under low operating pressure.
- Charge density of polyelectrolytes and surface potential of GO composite membranes jointly determine membranes' properties.

GRAPHICAL ABSTRACT

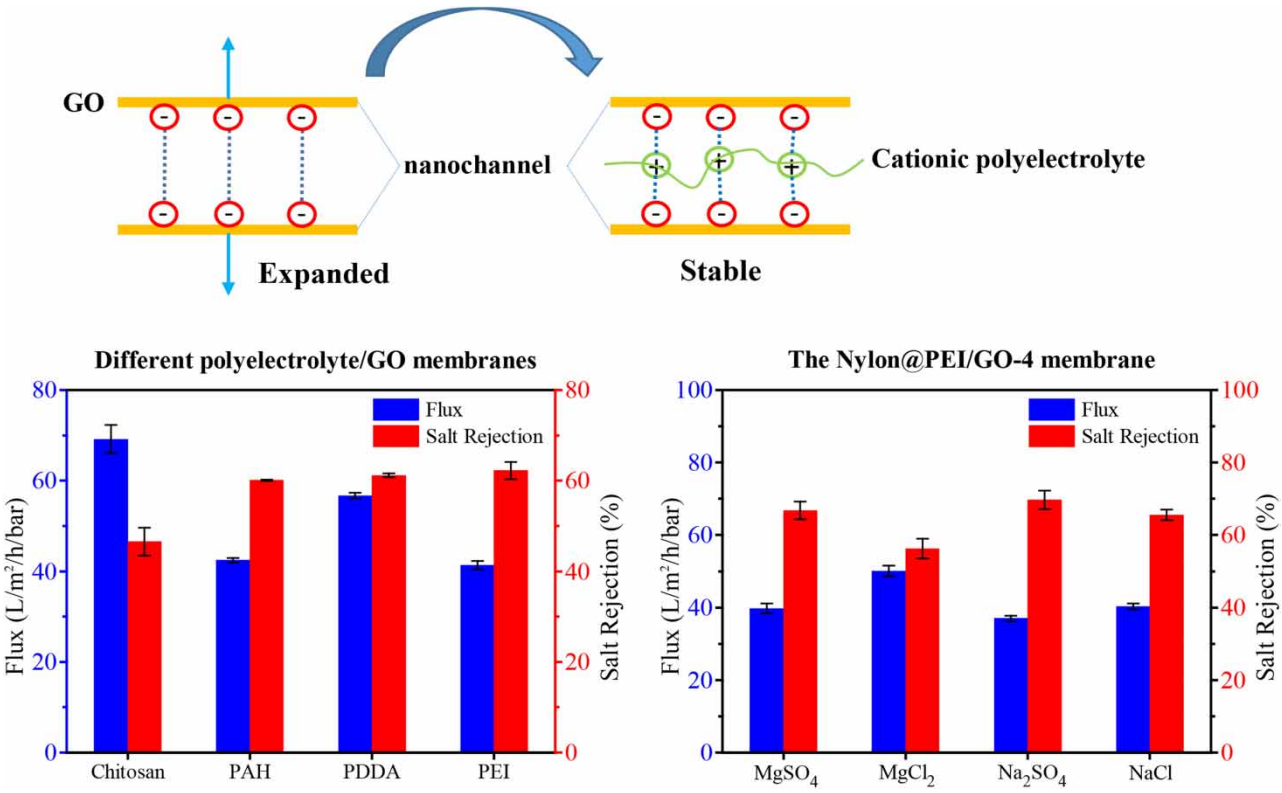

1. INTRODUCTION

Since Geim and Novoselov pioneered simple mechanical exfoliation to obtain single-layer graphene (Novoselov *et al.* 2004), graphene and its derived materials have rapidly become research hotspots in various fields. Graphene oxide (GO) derives from graphene oxidation, mainly composed of carbon atoms and polar oxygen-containing groups (such as hydroxyl, epoxy, and carboxyl) (Hung *et al.* 2014). As a typical two-dimensional material, GO is suitable for preparing a three-dimensional membrane by stacking GO nanosheets. In previous studies, GO membranes have shown great potential in water purification and desalination (Chen *et al.* 2017; Qian *et al.* 2019). What's more attractive is that it is convenient to prepare GO membranes with controllable thickness and composition through changing the preparation conditions (Mi 2014).

Nair *et al.* found that water vapor can transport quickly in the low-friction nanocapillaries formed between the non-oxidized regions of staked GO nanosheets, and other gases, including helium, cannot penetrate the GO membrane (Nair *et al.* 2012). Hu *et al.* suggested that water could flow through the nanochannels between GO layers while unwanted solutes are rejected by size exclusion and electrostatic repulsion (Hu & Mi 2013). However, hydration and electrostatic repulsion expand the interlayer spacing of GO nanosheets when immersed in water, making the GO membranes lose their ability to trap ions and small molecules with a hydration radius less than 0.45 nm (Joshi *et al.* 2014; Dong *et al.* 2020). Researchers have attempted to inhibit the swelling of GO in water based on different strategies, such as adding nanoparticles (Zhang *et al.* 2017), metal cations (Chen *et al.* 2017), or reduced graphene oxide (rGO) (Xi *et al.* 2016), epoxy encapsulation (Abraham *et al.* 2017), covalent modification (Jia *et al.* 2016; Qian *et al.* 2019; Zhang *et al.* 2019) etc.

The abundant oxygen-containing functional groups on the surface of GO make it negatively charged in the solution. Inspired by the self-assembly of polyelectrolyte membranes (PEMs) invented by Decher (Decher *et al.* 1992), cationic polyelectrolytes were introduced between GO nanosheets to improve the stability of GO membrane in solution via electrostatic interaction (Magnenet *et al.* 2012). Hu *et al.* fabricated a novel GO membrane by layer-by-layer (LbL) assembling negatively charged GO nanosheets on a porous poly(acrylonitrile) (PAN) supporter and interconnecting them with positively charged poly(allylamine hydrochloride) (PAH) via electrostatic attraction (Hu & Mi 2014). Wang *et al.* prepared a

poly(diallyldimethylammonium chloride) (PDDA)/GO multilayer membrane based on LbL self-assembly strategy, and its retention rate of methyl blue dye reached 99.2% (Wang *et al.* 2016). The interaction between GO nanosheets and polycations suppresses the swelling of the GO membranes and improves the stability of the composite membranes. On the other hand, the introduction of polycations strengthens the cation retention and anti-fouling performance of the composite membranes.

Researchers have been accustomed to using various ultrafiltration membranes as supporters in previous studies (Hu & Mi 2014; Wang *et al.* 2016), while few papers choose microfiltration (MF) membranes with a larger pore size as substrates. In this study, the nylon MF membrane with good chemical stability, acid and alkali resistance, and hydrophilicity is proposed as the supporter for the first time. Firstly, the larger pore size of the nylon membrane could guarantee a higher flux. Secondly, the hydrophilic nylon membrane is appropriate for use in water environments. To tailor the desalination performance of the GO membranes precisely, the effects of different preparation and operating conditions on the performance of the membrane are investigated. In addition, the effect of different cationic polyelectrolytes on the retention of low-valence ions in the GO composite membranes is reported.

2. EXPERIMENTAL

2.1. Materials and chemicals

Graphite (100 mesh) was purchased from Shanghai Titan Scientific Co., Ltd (China). poly(ethyleneimine) (PEI, Mw ~1,800), PDDA (Mw 100,000–200,000), PAH (Mw ~15,000) and chitosan were provided by Shanghai Aladdin Bio-Chem Technology Co., Ltd (China). The nylon MF membrane, whose average pore size is 0.22 μm, was obtained from Shanghai Xinya Purification Equipment Co., Ltd (China). The remaining reagents (analytical grade) were supplied by Shanghai Lingfeng Chemical Reagent Co., Ltd (China). Deionized (DI) water was self-made on campus, and its conductivity is lower than 2 μS/cm. All chemicals were used as received without further purification.

2.2. Preparation of GO membrane

High-quality GO was prepared to refer to the modified Hummers method (Han 2014) (see Text S1 in Supporting Information for more details). The nylon MF membrane was pre-treated first. A fresh nylon substrate was washed and dried at 50 °C, then dipped into the TEOS-ethanol (=1:15 vol) mixed solution, and then directly transferred to 1 M HCl. After reacting for 1 h, the substrate was washed and dried. The modified nylon supporter is negatively charged because of Si-OH and Si-O-Si bonds (Liu *et al.* 2019).

Finally, the modified nylon substrate was immersed in the cationic polyelectrolyte solution and the GO dispersion successively. Typically, the substrate was dipped into 1 mg/mL PEI for 30 min, and then immersed into 1 mg/mL GO dispersion for 30 min. After every immersion, the substrate was rinsed with DI water to remove excess adsorbent. Each time the above process was completed, it was recorded as a bilayer, and then the membrane was dried at 50 °C to enhance the toughness (Mamedov *et al.* 2002). Finally, the composite membrane was marked as Nylon@PEI/GO-n, where n represents the number of bilayers. The overall preparation process is illustrated in Figure 1.

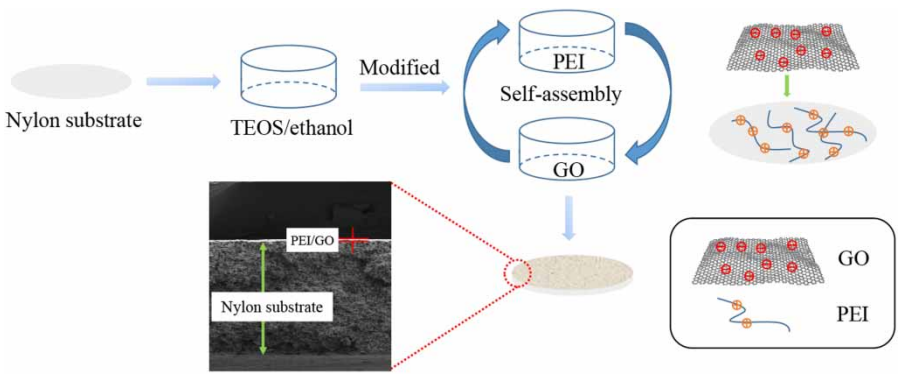

Figure 1 | LbL self-assembly of PEI/GO membrane on nylon substrate via electrostatic attraction.

2.3. Characterization

XRD spectra were obtained from a rotating anode X-ray powder diffractometer (D/max-2550VB, RIGAKU, Japan) with a monochromatized source of Cu $K_\alpha 1$ radiation at 4.0 kW (40 kV, 100 mA). Pristine graphite was analyzed using an FTIR spectrometer (Spectrum 100, PerkinElmer, USA). The functionalized groups of flake GO were detected by ATR-FTIR. Raman spectrum of graphite and GO were recorded by a Raman spectrometer (LabRam HR800, Horiba JobinYvon, France) at $\lambda = 532$ nm. The water contact angle of the membranes was determined by a contact angle tester (JY-82B Kruss DSA, Dataphysics, Germany). The assembly process of PEI/GO multilayers was monitored by a UV-vis spectrophotometer (UH4150, HITACHI, Japan). In order to obtain the UV-vis absorption spectrum, the PEI/GO composite membranes were deposited on the surface of the glass slides (see Text S2 for more details), which were treated by piranha solution in advance (Yu *et al.* 2006). The surface morphology of the composite membranes was observed by a scanning electron microscope (Nova NanoSEM 450, FEI, USA). The zeta potential was measured by an electrokinetic analyzer (Surpass, Anton-Paar, Austria) with a clamping cell at 300 mbar, and 1.0 mM KCl was used as the electrolyte solution.

2.4. Desalination testing of composite membrane

The desalination performance of membranes was carried out in a lab-made dead-end filtration test system (Figure S1) with an effective area of 12.57 cm^2, and the transmembrane pressure was maintained at 1 bar. The filtrate was collected through the container below, and the volume of the filtrate was measured directly.

The permeation flux (J) and rejection (R) were determined under steady-state conditions. The permeation flux, J, was calculated by

$$J = \frac{V}{A \cdot t \cdot \Delta P} \tag{1}$$

where V is the volume (L) of permeate collected on a time scale t (h) under the transmembrane pressure ΔP (bar), and A is the effective area of the composite membrane (m^2). The rejection, R, was calculated by

$$R = 1 - \frac{K_p}{K_f} \times 100\% \tag{2}$$

where K_p and K_f are the conductivity (μS/cm) of feed and permeate, respectively. The conductivity was determined by a conductivity meter (DDS-11A, Shanghai REX, China). During all experiments, the concentration of the feed solution was not higher than 1 mg/mL, so the conductivity was considered to be approximately proportional to the concentration. Thus, the conductivity was directly used to calculate rejection instead of the concentration.

3. RESULTS AND DISCUSSION

3.1. Characterization of GO and graphite

Figure 2(a) shows the XRD spectra of GO and pristine graphite. Graphite has a characteristic peak at $2\theta = 26.5°$, and the characteristic peak of GO occurs at $2\theta = 10.3°$. The calculated d-spacing of pristine graphite and GO are 0.34 nm and

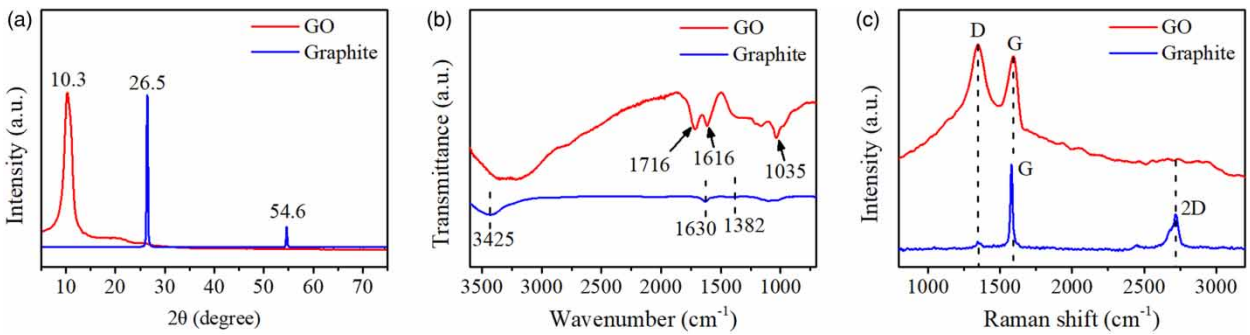

Figure 2 | Characterization of GO and pristine graphite. (a) XRD spectra, (b) infrared spectra, and (c) Raman spectra, respectively.

0.86 nm, respectively. The above characterization results are consistent with those reported in other literature (Shin *et al.* 2009). Water molecules and oxygen-containing functional groups are introduced into the carbon atom layer of raw graphite with the interaction of oxidants ($KMnO_4$), which causes the layer to wrinkle and the layer spacing increases along the *c*-axis (Wang *et al.* 2008).

As a stable form of carbon, graphite usually has no significant peaks in the infrared spectrum. However, the adsorption of water vapor in the air and impurities introduced during the production process causes some weak peaks in the spectrum of graphite (Tucureanu *et al.* 2016). Figure 2(b) shows the adsorption peaks of pristine graphite and GO. The peaks of graphite at 3,425 cm^{-1} and 1,630 cm^{-1} are contributed to the adsorbed water. Nitric acid molecules may insert into the graphite in the production process, which causes a weak peak attributed to NO_3^- that could be observed at 1,382 cm^{-1} (Zhang *et al.* 2011). The broad peak at 3,000–4,000 cm^{-1} of GO is caused by the stretching vibration of the hydroxyl group. The peaks at 1,716 cm^{-1} and 1,157 cm^{-1} are contributed to the stretching vibration of C = O and C-O in the carboxyl group. The stretching vibration of C-O in the epoxy group is observed at 1,208 cm^{-1} and 1,035 cm^{-1}. The peak at 1,616 cm^{-1} is not easy to identify because it may correspond to the bending vibration of the hydroxyl group or the in-plane vibration of C = C. These analysis results are similar to other articles (Dumee *et al.* 2014; Zahed & Hosseini-Monfared 2015).

The conjugated C = C bond in carbon materials causes strong Raman signals, thus the latter is usually used for characterization and analysis of these materials. As shown in Figure 2(c), the G peak and 2D peak of graphite are detected at 1,580 cm^{-1} and 2,716 cm^{-1}, respectively. The G peak contributed to in-plane vibration of sp^2 hybridized carbon atoms. The 2D peak only appears in defect-free graphite (Nemanich & Solin 1979). The D peak of GO, located at 1,358 cm^{-1}, is absent from defect-free graphene but exists in defected graphene. The 2D peak in graphite shows no obvious defect in graphite, and its microstructure is relatively regular. Meanwhile, the D peak appeared, and the 2D peak disappeared in GO, indicating that after oxidation, significant defect sites appeared in the hexagonal honeycomb structure of the original graphene.

3.2. Characterization of GO membrane

Two peaks of GO are located at 230 and 300 nm in the UV-vis spectrum, corresponding to the aromatic C-C bond and C = O bond, respectively (Paredes *et al.* 2008). Meanwhile, the maximum absorption peak of PEI appears at 202 nm (Figure 3(a)). With the LbL stacking of the composite membranes, the concentration of corresponding functional groups increases continuously, which leads to the change in the intensity of characteristic peaks at 230 and 300 nm. As shown in Figure 3(b), the absorption intensity increases with the increase of the bilayer number of GO membranes. The absorbance of characteristic peaks located at 230 and 300 nm are plotted against the bilayer number, respectively. It is obvious that the absorbance is linearly related to the bilayer number, which fully proves that PEI/GO composite membranes with different bilayers have been successfully prepared by the LbL self-assembly method.

In the infrared spectrum of the nylon membrane (Figure 4), the peak at 3,290 cm^{-1} corresponds to the absorption of $-NH_2$, the peaks at 2,930 cm^{-1} and 2,863 cm^{-1} belong to $-CH_2-$, the absorption peak at 1,632 cm^{-1} is caused by the stretching vibration of C = O, and the peak at 1,536 cm^{-1} is derived from the deformation vibration of N–H. As the nylon substrate has several strong absorption peaks from 3,360 cm^{-1} to 1,500 cm^{-1}, the infrared spectrum of Nylon@PEI/GO-4 is similar

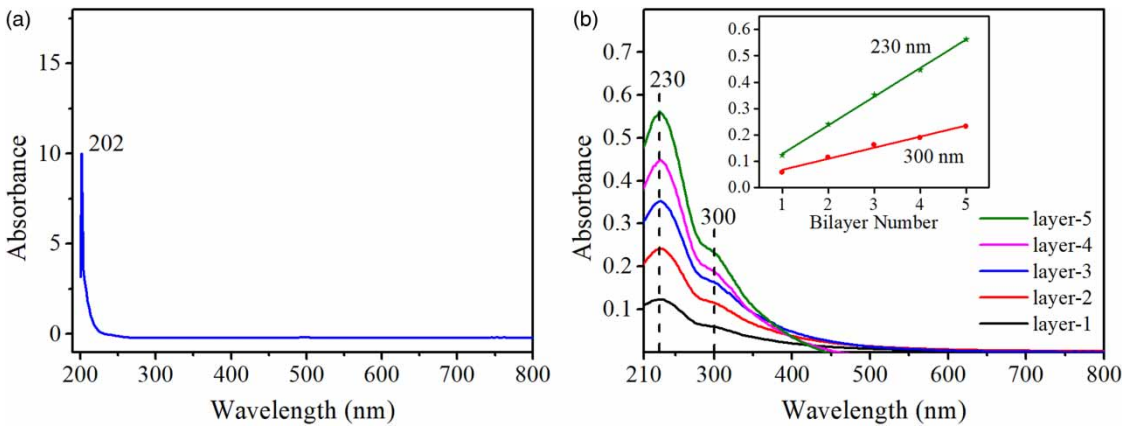

Figure 3 | UV-vis spectra. (a) 1 mg/mL PEI aqueous solution; (b) PEI/GO composite membranes with different bilayer numbers.

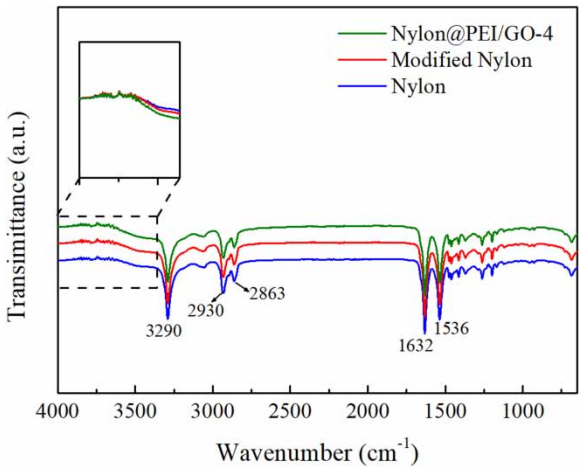

Figure 4 | ATR-FTIR spectra of nylon substrate, modified nylon and the Nylon@PEI/GO composite membrane.

to those of the supporter, which is consistent with another report (Halakoo & Feng 2020). From 3,600 cm^{-1} to 3,360 cm^{-1}, the peak intensity of the modified nylon substrate and the GO composite membrane gradually increased, indicating that the amount of hydroxyl increased, which is attributed to the modification of the nylon membrane and the loaded GO membrane, respectively.

The surface hydrophilicity of the nylon membrane changes after being modified and loading of the GO layer (Figure S2). The water contact angle of the nylon MF membrane is 38.6°, indicating that nylon has good hydrophilicity. After being modified, the angle increases to 44.3°, which may be related to the hydroxyl group density on the surface of the modified nylon membrane. When the PEI/GO bilayer is deposited, the angle continues to rise to 51.1°. Oxygen-containing functional groups (hydroxyl and carboxyl groups) on the surface of GO nanosheets show great hydrophilicity, but sp^2 carbon atoms in the unoxidized region of GO exhibit hydrophobicity. With the continuous deposition of PEI/GO, the final hydrophilicity of the composite membrane decreased slightly, but the membranes were still hydrophilic.

SEM was used to observe the surface morphology of the Nylon@PEI/GO membrane. There are numerous wrinkles on the membrane's surface (Figure S3a), which increase the contact area between the feed solution and the membrane. On the other hand, folds may also lead to membrane cracking (Figure S3b), which leads to the degradation of desalination performance. Ultimately, the desalination performance of the GO membrane is a balance between the above two aspects.

3.3. Influence of preparation conditions

The preceding content confirms that the cationic polyelectrolyte/GO composite membrane has been successfully prepared. Then the influence of preparation and operation conditions on the desalination performance of composite membranes was investigated. In order to eliminate the interference of the nylon substrate, the retention of fresh nylon membrane and modified membrane were tested with 0.01 g/L $MgSO_4$ feed solution. It is considered that the substrates adopted in the experiments have no contribution to the desalination because the salt rejection of the above two membranes is close to 0%.

With other experimental conditions unchanged, the composite membranes with different bilayers were prepared and evaluated, respectively. As shown in Figure 5(a), when the bilayer number is 1 or 2, GO nanosheets cannot completely cover the nylon supporter, so the flux is high, and the retention rate is low. After the third bilayer is assembled, the flux drops drastically, and the desalination rate rises rapidly. In particular, the salt rejection of Nylon@PEI/GO-4 reaches 56.7% for 0.01 g/L $MgSO_4$ feed solution, and the solution flux is maintained at 83.7 $L{\cdot}m^{-2}{\cdot}h^{-1}{\cdot}bar^{-1}$. Interestingly, after being assembled to the fifth bilayer, the rejection of the GO membrane decreases slightly. According to previous studies, there is no obvious positive correlation relationship between the bilayer number and hydraulic resistance of the GO membrane, which is speculated to be related to the water transmission characteristics in nanochannels between GO nanosheets (Hu & Mi 2013, 2014). Similarly, this phenomenon is also observed in CNT films (Cohen-Tanugi & Grossman 2012).

Figure 5(b) shows the effect of PEI concentration. The bilayer number was specified as 4, and the concentration of PEI was adjusted from 0.5 to 2.5 g/L. With the increase of PEI concentration within the experimental range, both water flux (Figure S4b) and salt solution flux decrease first and then increase rapidly. This might be related to the effect of PEI

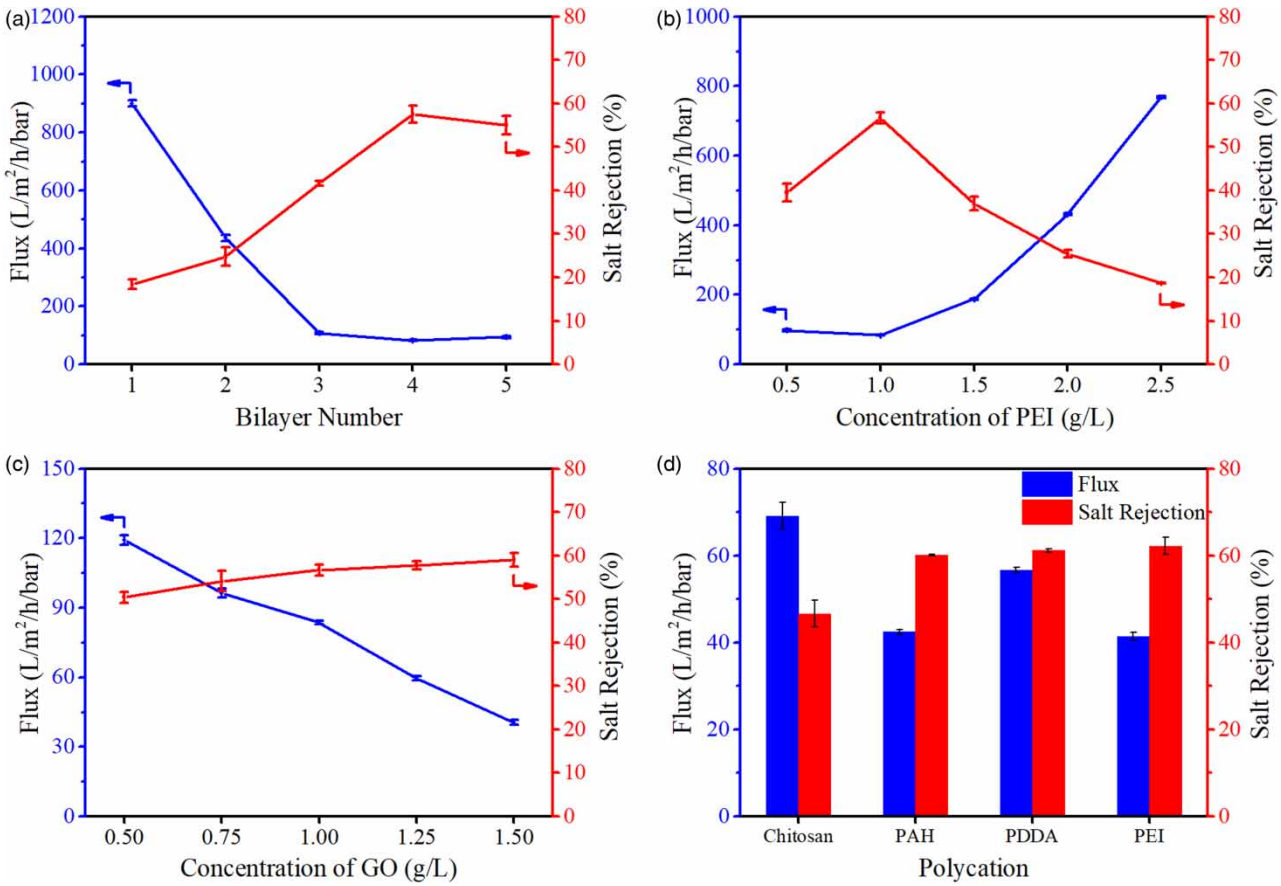

Figure 5 | Influence of preparation conditions on the performance of Nylon@PEI/GO membrane for 0.01 g/L $MgSO_4$. (a) bilayer number; (b) concentration of PEI; (c) concentration of GO; (d) cationic polyelectrolyte types.

concentration on its molecular chain morphology (Gao *et al.* 2017). When PEI concentration is low, polyelectrolyte chains appear as stretched linear, and the charge density of cross-linking is high, which makes the composite membrane exhibit a high retention rate. After concentration increases to a certain value, the chain gradually changes from uncoiled to contracted spherical coils under the effect of electrostatic repulsion. Finally, PEI macromolecules are adsorbed on the GO nanosheets' surface in the form of coils, resulting in a decrease in charge density and recombination. Thus, the permeability decreases accordingly. The variation trend of the surface zeta potential of the composite membranes under different PEI concentrations (see Table S1 in Supplementary Material) is consistent with the desalination rate, indicating that the ion retention ability of the cationic polyelectrolyte/GO composite membrane is mainly determined by the electrostatic repulsion between the negatively charged membrane and the ions.

Figure 5(c) shows the effect of GO concentration. With the increase of GO concentration from 0.5 to 1.5 g/L, flux decreases, and salt rejection increases correspondingly. Within the experimental range, the maximum salt retention is 59.0%. It is considered that with the increase of GO concentration, the thickness of the functional bilayer increases, and the permeability resistance increases correspondingly. The removal rate for 0.01 g/L $MgSO_4$ only increases from 50.4 to 59.0% within the experimental range. On the other hand, the concentration of GO dispersion is generally lower than 10 mg/mL. The stability of the dispersion decreases with the increase of concentration. It's uneconomical to sacrifice the stability of the GO dispersion to improve the desalination performance slightly.

The charge density of a polyelectrolyte refers to the ratio of the number of ions contained in the repeating unit to the number of carbon atoms. Different PEMs have different structures due to different charge densities (Miller & Bruening 2004). In addition to PEI, PDDA, PAH and chitosan were used to assemble the GO membrane, and the desalination performance was measured with 0.01 g/L $MgSO_4$. Figure 5(d) shows that the salt solution flux of different composite membranes is: PEI/GO < PAH/GO < PDDA/GO < chitosan/GO, which is consistent with the charge density of these polycations (PEI >

PAH > PDDA > chitosan) (Miller & Bruening 2004; Wang *et al.* 2016). The higher the charge density of polycation is, the higher the cross-linking density is, which makes the GO membrane tighter, so the flux decreases. The desalination rate to 0.01 g/L $MgSO_4$ of different cationic polyelectrolyte/GO composite nanofiltration membranes were 62.2% (Nylon@PEI/GO-4), 61.2% (Nylon@PDDA/GO-4), 60.1% (Nylon@PAH/GO-4), and 46.6% (Nylon@Chitosan/GO-4), respectively. The experiment results show that Nylon@PEI/GO-4 has the highest salt rejection efficiency. The surface zeta potential of these four GO membranes (see Table S2 in Supplementary Material) shows that they are all negatively, and Nylon@PEI/GO-4 has the strongest electronegativity. According to the Donnan effect, negatively charged membranes have a stronger repulsive force towards high-valence anions. Therefore, Nylon@PEI/GO-4 obtained the best salt rejection performance for $MgSO_4$.

3.4. Influence of operating conditions

After exploring the effect of different preparation conditions on GO membranes' performance, the operating conditions were investigated. When the concentration of $MgSO_4$ rises from 0.01 to 1.0 g/L, the flux decreases, and the rejection rate increases slightly, respectively (Figure 6(a)). Particularly, the desalination rate of the Nylon@PEI/GO-4 reaches 66.8% for 1.0 g/L $MgSO_4$, and the flux maintains at 39.8 $L{\cdot}m^{-2}{\cdot}h^{-1}{\cdot}bar^{-1}$. Although the single-pass retention rate of the prepared GO composite membrane for low-valence salt solutions is less than 70%, which is similar to 69.2% (Wang *et al.* 2016) but lower than 93.9% (Nan *et al.* 2016). The nanofiltration membrane presents an obvious trade-off between flux and retention. Compared with the above literature, the flux obtained in this study is 6–9 times more than their results (6.95 $L{\cdot}m^{-2}{\cdot}h^{-1}{\cdot}bar^{-1}$ for Wang, and 4.16 $L{\cdot}m^{-2}{\cdot}h^{-1}{\cdot}bar^{-1}$ for Nan).

Before the cationic polyelectrolyte is introduced, the GO membrane immersed into the salt solution will be subjected to three kinds of forces: (1) F_a, the pressure on nanochannels from the salt solutions (Huang *et al.* 2013); (2) F_b, the electrostatic repulsion of negative charges on GO surface; (3) F_c, swelling caused by intercalation of water molecules (see in Figure 7). The

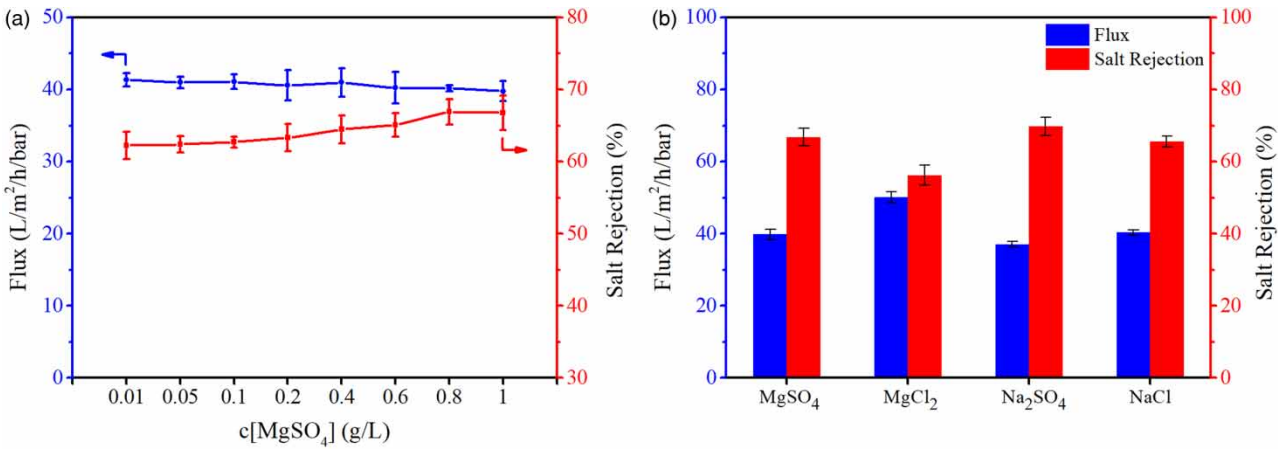

Figure 6 | Influence of operating conditions on the performance of Nylon@PEI/GO-4 membrane. (a) $MgSO_4$; (b) 1.0 g/L salt solutions.

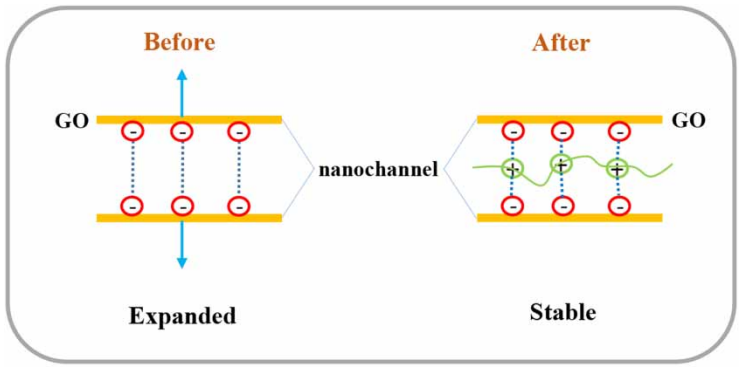

Figure 7 | Nanochannels before and after cross-linking.

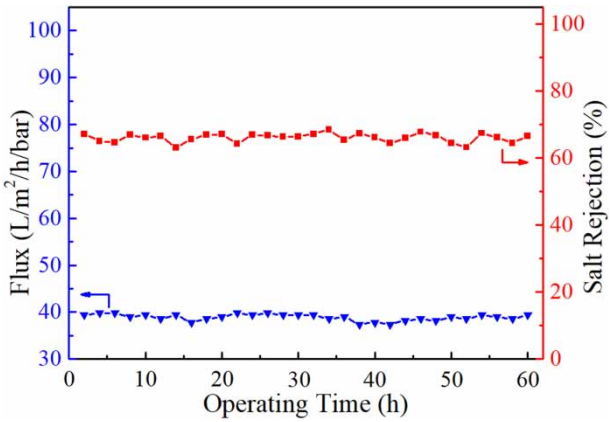

Figure 8 | Influence of salt concentration on the performance of the Nylon@PEI/GO-4 membrane.

ultimate performance of the GO membrane is to reduce or even lose the retention of salt ions (Joshi *et al.* 2014; Dong *et al.* 2020), indicating that F_b and F_c are greater than F_a, which results in nanochannels expanding. After the introduction of the polycation, F_b changes from electrostatic repulsion to electrostatic attraction, which effectively inhibits the swelling of the GO membrane. That is, F_b and F_c partly cancel each other. With the increase of salt ion concentration, F_a also increases and compresses nanochannels, leading to an upward trend in the rejection rate.

The charged nanofiltration membrane shows better retention performance on high-valence homonymous ions and exhibits a low rejection rate on high-valence counter ions due to the charge shielding effect (Han *et al.* 2013). Four typical inorganic salts ($MgSO_4$, $MgCl_2$, Na_2SO_4 and NaCl) were selected, and the desalination performance of the Nylon@PEI/GO-4 to the above salt solutions was determined. As shown in Figure 6(b), the salt retention rate of the GO membrane for four different salt solutions varied according to $Na_2SO_4 > MgSO_4 \approx NaCl > MgCl_2$. According to the Donnan mechanism, the negatively charged GO composite membrane has a stronger repulsive force against high-valence anion (SO_4^{2-}). On the other hand, the high-valence cation (Mg^{2+}) has a charge shielding effect, which leads to a decrease in the retention of GO membranes. Therefore, the cation polyelectrolyte/GO composite membrane has the highest rejection rate of Na_2SO_4 and the lowest retention rate of $MgCl_2$ in theory. The c(SO_4^{2-}) (molarity) in $MgSO_4$ is only half of c(Cl^-) in NaCl, and Mg^{2+} has a stronger charge shielding effect than Na^+, leading to a similar rejection rate of the cation polycation/GO composite membranes to the $MgSO_4$ and NaCl.

3.5. Stability of GO membrane

The GO membrane's stability in long time running was also examined via a 60 h filtration test. As shown in Figure 8, the Nylon@PEI/GO-4 maintained stability with the 60-hour experimental range. On average, the flux was maintained at 38.9 $L{\cdot}m^{-2}{\cdot}h^{-1}{\cdot}bar^{-1}$, and the retention rate was kept at 66.1%. The newly introduced cationic polyelectrolyte forms electrostatic attraction with the negative charge on GO nanosheets' surface, which effectively counteracts the swelling effect, thus ensuring the stability of nanochannels in the GO membrane.

4. CONCLUSION

In this study, the cationic polyelectrolyte/GO composite membranes were fabricated by LbL self-assembly via electrostatic attraction based on nylon MF membranes. By adjusting the concentration of feed solution within a certain range, the GO membranes show stable desalination performance, indicating that the introduction of polycations effectively improves the composite membranes' stability. For four specific salt solutions, the order of retention rate is $Na_2SO_4 > MgSO_4 \approx NaCl > MgCl_2$, consistent with the characteristics of negatively charged nanofiltration membrane. The investigation results of various cationic polyelectrolytes show that the polyelectrolytes' charge density and the surface potential of the composite membranes jointly determine the membranes' properties. Due to the simple and thin membrane structure and relatively large pore of the MF supporter, the GO composite membrane obtains considerable desalination performance while maintaining high flux. Typically, the salt rejection rate of the Nylon@PEI/GO-4 reaches 66.8% for 1.0 g/L $MgSO_4$, and the flux maintains at 39.8 $L{\cdot}m^{-2}{\cdot}h^{-1}{\cdot}bar^{-1}$. Benefitting from the composite membrane maintaining similar retention for both high and low

concentration salt solutions, the ideal desalination performance could be obtained through multi-stage processes on the premise of ensuring high flux, which is obviously more suitable for industry.

DATA AVAILABILITY STATEMENT

All relevant data are included in the paper or its Supplementary Information.

REFERENCES

Abraham, J., Vasu, K. S., Williams, C. D., Gopinadhan, K., Su, Y., Cherian, C. T., Dix, J., Prestat, E., Haigh, S. J., Grigorieva, I. V., Carbone, P., Geim, A. K. & Nair, R. R. 2017 Tunable sieving of ions using graphene oxide membranes. *Nat. Nanotechnol.* **12**, 546–550. doi:10.1038/NNANO.2017.21.

Chen, L., Shi, G. S., Shen, J., Peng, B. Q., Zhang, B. W., Wang, Y. Z., Bian, F. G., Wang, J. J., Li, D. Y., Qian, Z., Xu, G., Liu, G. P., Zeng, J. R., Zhang, L. J., Yang, Y. Z., Zhou, G. Q., Wu, M. H., Jin, W. Q., Li, J. Y. & Fang, H. P. 2017 Ion sieving in graphene oxide membranes via cationic control of interlayer spacing. *Nature* **550**, 380–383. doi:10.1038/nature24044.

Cohen-Tanugi, G. & Grossman, J. C. 2012 Water desalination across nanoporous graphene. *Nano Lett.* **12** (7), 3602–3608. doi:10.1021/nl3012853.

Decher, G., Hong, J. D. & Schmitt, J. 1992 Buildup of ultrathin multilayer films by a self-assembly process: III. consecutively alternating adsorption of anionic and cationic polyelectrolytes on charged surfaces. *Thin Solid Films* **210–211**, 831–835. doi:10.1016/0040-6090(92)90417-A.

Dong, Y. P., Lin, C., Gao, S. J., Manoranjan, N., Li, W. X., Fang, W. X. & Jin, J. 2020 Single-layered GO/LDH hybrid nanoporous membranes with improved stability for salt and organic molecules rejection. *J. Membrane. Sci.* **607**, 118184. doi:10.1016/j.memsci.2020.118184.

Dumee, L. F., Feng, C. F., He, L., Allioux, F. M., Yi, Z. F., Gao, W. M., Banos, C., Davies, J. B. & Kong, L. X. 2014 Tuning the grade of graphene: gamma ray irradiation of free-standing graphene oxide films in gaseous phase. *Appl. Surf. Sci.* **322**, 126–135. doi:10.1016/j.apsusc.2014.10.070.

Gao, K., Xu, Z. H., Hong, Y. B., Ding, M. T., He, X. M. & Lan, W. G. 2017 Layer-by-layer self-assembly preparation and performance of GO-ceramics composite nanofiltration membrane. *J. Chem. Ind. Eng. (China)* **68** (5), 2178–2185 (in chinese).

Halakoo, E. & Feng, X. S. 2020 Self-assembled membranes from polyethylenimine and graphene oxide for pervaporation dehydration of ethylene glycol. *J. Membrane Sci.* **616**, 118583. doi:10.1016/j.memsci.2020.118583.

Han, Y. 2014 *Preparation, Modification and Performance Study of Graphene Nanofiltration Membrane*. PhD thesis, Zhejiang University, Hangzhou, China.

Han, Y., Xu, Z. & Gao, C. 2013 Ultrathin graphene nanofiltration membrane for water purification. *Adv. Funct. Mater.* **23** (29), 3693–3700. doi:10.1002/adfm.201202601.

Hu, M. & Mi, B. X. 2013 Enabling graphene oxide nanosheets as water separation membranes. *Environ. Sci. Technol.* **47** (8), 3715–3723. doi:10.1021/es400571 g.

Hu, M. & Mi, B. X. 2014 Layer-by-layer assembly of graphene oxide membranes via electrostatic interaction. *J. Membrane Sci.* **469**, 80–87. doi:10.1016/j.memsci.2014.06.036.

Huang, H. B., Mao, Y. Y., Ying, Y. L., Liu, Y., Sun, L. W. & Peng, X. S. 2013 Salt concentration, pH and pressure controlled separation of small molecules through lamellar graphene oxide membranes. *Chem. Commun.* **49** (53), 5963–5965. doi:10.1039/c3cc41953c.

Hung, W. S., Tsou, C. H., Guzman, M. D., An, Q. F., Liu, Y. L., Zhang, Y. M., Hu, C. C., Lee, K. R. & Lai, J. Y. 2014 Cross-linking with diamine monomers to prepare composite graphene oxide-framework membranes with varying d-spacing. *Chem. Mater.* **26** (9), 2983–2990. doi:10.1021/cm5007873.

Jia, Z. Q., Wang, Y., Shi, W. X. & Wang, J. L. 2016 Diamines cross-linked graphene oxide free-standing membranes for ion dialysis separation. *J. Mater. Chem. A* **520**, 139–144. doi:10.1016/j.memsci.2016.07.042.

Joshi, R. K., Carbone, P., Wang, F. C., Kravets, V. G., Su, Y., Grigorieva, I. V., Wu, H. A., Geim, A. K. & Nair, R. R. 2014 Precise and ultrafast molecular sieving through graphene oxide membranes. *Science* **343** (6172), 752–754. doi:10.1126/science.1245711.

Liu, W., Li, H. J., Jin, J. L., Wang, Y. Z., Zhang, Z., Chen, Z. D., Wang, Q., Chen, Y. G., Paek, E. & Mitlin, D. 2019 Synergy of epoxy chemical tethers and defect-free graphene in enabling stable lithium cycling of silicon nanoparticles. *Angew. Chem. Int. Edit.* **58** (46), 16590–16600. doi:10.1002/anie.201906612.

Magnenet, C., Lakard, S., Buron, C. C. & Lakard, B. 2012 Functionalization of organic membranes by polyelectrolyte multilayer assemblies: application to the removal of copper ions from aqueous solutions. *J. Colloid Interf. Sci.* **376**, 202–208.

Mamedov, A. A., Kotov, N. A., Prato, M., Guldi, D. M., Wicksted, J. P. & Hirsch, A. 2002 Molecular design of strong single-wall carbon nanotube/polyelectrolyte multilayer composites. *Nat. Mater.* **1**, 190–194. doi:10.1038/nmat747.

Mi, B. X. 2014 Graphene oxide membranes for ionic and molecular sieving. *Science* **343** (6172), 740–742. doi:10.1126/science.1250247.

Miller, M. D. & Bruening, M. L. 2004 Controlling the nanofiltration properties of multilayer polyelectrolyte membranes through variation of film composition. *Langmuir* **20**, 11545–11551. doi:10.1021/la0479859.

Nair, R. R., Wu, H. A., Jayaram, P. N., Grigorieva, I. V. & Geim, A. K. 2012 Unimpeded permeation of water through helium-leak–tight graphene-based membranes. *Science* **335** (6067), 442–444. doi:10.1126/science.1211694.

Nan, Q., Li, P. & Cao, B. 2016 Fabrication of positively charged nanofiltration membrane via the layer-by-layer assembly of graphene oxide and polyethylenimine for desalination. *Appl. Surf. Sci.* **387**, 521–528. doi:10.1016/j.apsusc.2016.06.150.

Nemanich, J. & Solin, S. A. 1979 First- and second-order Raman scattering from finite-size crystals of graphite. *Phys. Rev. B* **20** (2), 392–401. doi:10.1103/PhysRevB.20.392.

Novoselov, K. S., Geim, A. K., Morozov, S. V., Jiang, D., Zhang, Y., Dubonos, S. V., Grigorieva, I. V. & Firsov, A. A. 2004 Electric field effect in atomically thin carbon films. *Science* **306** (5696), 666–669. doi:10.1126/science.1102896.

Paredes, J. I., Villar-Rodil, S., Martinez-Alonso, A. & Tascon, J. M. D. 2008 Graphene oxide dispersions in organic solvents. *Langmuir* **24** (19), 10560–10564. doi:10.1021/la801744a.

Qian, Y. L., Zhang, X. L., Liu, C. Y., Zhou, C. & Huang, A. S. 2019 Tuning interlayer spacing of graphene oxide membranes with enhanced desalination performance. *Desalination* **460**, 56–63. doi:10.1016/j.desal.2019.03.009.

Shin, H. J., Kim, K. K., Benayad, A., Yoon, S. M., Park, H. K., Jung, I. S., Jin, M. H., Jeong, H. K., Kim, J. M., Choi, J. Y. & Lee, Y. H. 2009 Efficient reduction of graphite oxide by sodium borohydride and its effect on electrical conductance. *Adv. Funct. Mater.* **19** (12), 1987–1992. doi:10.1002/adfm.200900167.

Tucureanu, V., Matei, A. & Avram, A. M. 2016 FTIR spectroscopy for carbon family study. *Anal. Chem.* **46** (6), 502–520. doi:10.1080/10408347.2016.1157013.

Wang, G. X., Yang, J., Park, J., Gou, X. L., Wang, B., Liu, H. & Yao, J. 2008 Facile synthesis and characterization of graphene nanosheets. *J Phys. Chem. C* **112** (22), 8192–8195. doi:10.1021/jp710931 h.

Wang, L., Wang, N. X., Li, J., Li, J. W., Bian, W. Q. & Ji, S. L. 2016 Layer-by-layer self-assembly of polycation/GO nanofiltration membrane with enhanced stability and fouling resistance. *Sep. Purif. Technol.* **160**, 123–131. doi:10.1016/j.seppur.2016.01.024.

Xi, Y. H., Hu, J. Q., Liu, Z., Xie, R., Ju, X. J., Wang, W. & Chu, L. Y. 2016 Graphene oxide membranes with strong stability in aqueous solutions and controllable lamellar spacing. *ACS Appl Mater. Inter.* **8** (24), 15557–15566. doi:10.1021/acsami.6b00928.

Yu, H. H., Cao, T., Zhou, L. D., Gu, E. D., Yu, D. S. & Jiang, D. S. 2006 Layer-by-layer assembly and humidity sensitive behavior of poly(ethyleneimine)/multiwall carbon nanotube composite films. *Sensor Actuat. B-Chem.* **119** (2), 512–515. doi:10.1016/j.snb.2005.12.048.

Zahed, B. & Hosseini-Monfared, H. 2015 A comparative study of silver-graphene oxide nanocomposites as a recyclable catalyst for the aerobic oxidation of benzyl alcohol: support effect. *Appl. Surf. Sci.* **328**, 536–547. doi:10.1016/j.apsusc.2014.12.078.

Zhang, S. T., Gu, A. Y., Gao, H. F. & Che, X. Q. 2011 Characterization of exfoliated graphite prepared with the method of secondary intervening. *Int. J. Ind. Chem.* **2** (2), 123–130.

Zhang, M. C., Guan, K. C., Shen, J., Liu, G. P., Fan, Y. Q. & Jin, W. Q. 2017 Nanoparticles@rGO membrane enabling highly-enhanced water permeability and structural stability with preserved selectivity. *AlChE J.* **63** (11), 5054–5063. doi:10.1002/aic.15939.

Zhang, Y., Huang, L. J., Wang, Y. X., Tang, J. G., Wang, Y., Cheng, M. M., Du, Y. C., Yang, K., Kipper, M. J. & Hedayati, M. 2019 The preparation and study of ethylene glycol-modified graphene oxide membranes for water purification. *Polymers* **11**, 188–199. doi:10.3390/polym11020188.

First received 19 February 2021; accepted in revised form 14 August 2021. Available online 26 August 2021